

## Polycarbonate nanocomposites: Part 2. Degradation and color formation

P.J. Yoon<sup>a</sup>, D.L. Hunter<sup>b</sup>, D.R. Paul<sup>a,\*</sup>

<sup>a</sup>Department of Chemical Engineering and Texas Materials Institute, The University of Texas at Austin, Austin, TX 78712-1065, USA

<sup>b</sup>Southern Clay Products, 1212 Church St., Gonzales, TX 78629, USA

Received 11 March 2003; received in revised form 6 June 2003; accepted 9 June 2003

---

### Abstract

Polycarbonate nanocomposites were prepared using two different twin screw extruders from a series of organoclays based on sodium montmorillonite, with somewhat high iron content, exchanged with various amine surfactants. It seems that a longer residence time and/or broader residence time distribution are more effective for dispersing the organoclay. The effects of organoclay structure on color formation during melt processing were quantified using colorimeter and UV–Vis spectroscopy techniques. Color formation in the PC nanocomposites depends on the type of organoclay and the type of pristine clay employed. Double bonds in the hydrocarbon tail of the surfactants lead to more darkly colored materials than saturated surfactants. The most severe color was observed when using a surfactant containing hydroxy-ethyl groups and a hydrocarbon tail derived from tallow. Molecular weight degradation of the PC matrix during melt processing produces phenolic end groups which were tracked by UV–Vis spectroscopy. Greater dispersion of the clay generally led to higher reduction in molecular weight due to the increased surface area of clay exposed; however, for color, the situation is far more complex. Hydroxy-ethyl groups and tallow unit on the surfactant lead to more degradation. A selected series of organoclays based on synthetic clay Laponite® and calcium montmorillonite from Texas (TX-MMT) were also prepared to explore the effects of the clay structure. Laponite® and TX-MMT produce less color formation in PC nanocomposites than montmorillonite probably due to lower content of iron. Dynamic rheological properties support the trends of molecular weight degradation and dispersion of clay.

© 2003 Elsevier Ltd. All rights reserved.

**Keywords:** Polycarbonate; Nanocomposites; Melt processing

---

### 1. Introduction

The previous paper described the effects of organoclay structure on the morphology and mechanical properties of polycarbonate-based nanocomposites formed by melt processing [1]. The level of stiffness enhancement achieved strongly depends on the surfactant used to prepare the organoclay from sodium montmorillonite; however, for all organoclays, the degree of exfoliation of the layered aluminosilicate in the polycarbonate matrix was found to be much less than reported previously for nylon 6 using similar processing procedures [2].

Polycarbonate is susceptible to a variety of chemical processes caused by thermal and oxidative degradation mechanisms at elevated temperatures during melt processing [3–13]; these reactions may be significantly exacerbated by the addition of well-dispersed nanofillers. A

specific concern is that the ammonium alkyl surfactants in the organoclay undergo complex degradation reactions at 180 °C and higher [14,15]. In addition, a variety of metal ions exist in natural clays [16,17], and the degradation products of these constituents may trigger various reactions and color formation processes in polycarbonate.

The objective of this study is to explore some of these chemical issues, including degradation and color formation, and the influence of various processing variables during melt processing for polycarbonate-based nanocomposites. In addition to organoclays based on the sodium montmorillonite, synthetic clays were also used in this work to explore how clay constituents affect the chemical processes that occur during melt processing of polycarbonate-based nanocomposites. The extent of color formation and polymer matrix degradation for injection molded polycarbonate nanocomposite specimens formed from various organoclays by two twin screw extruders are documented in this paper using various analytical techniques.

---

\* Corresponding author. Tel.: +1-512-471-5392; fax: +1-512-471-0542.  
E-mail address: [drp@che.utexas.edu](mailto:drp@che.utexas.edu) (D.R. Paul).

## 2. Background

On extended exposure at elevated temperature, Bisphenol A polycarbonate degrades and turns progressively more yellow. Over the years, there have been numerous studies to understand these degradative processes with a special emphasis on identifying the chemical species responsible for the observed yellow color [3–13]. These studies suggest that thermal degradation of polycarbonates can proceed by chain scission [4–6]. In this process, major by-products of the thermal degradation of polycarbonate are phenol, bisphenol A, isopropenyl phenol, *p*-cresol, or diphenyl carbonate. Subsequently, these chemicals can react with polycarbonate molecules or be converted to various quinone compounds that could be one of the potential sources of yellow color in degraded polycarbonates [12].

Smith et al. observed severe color formation during melt blending of polycarbonate with a copolyester caused by the interaction of residual titanium catalyst in the copolyester with phenolic end groups of the polycarbonate [18]. Naturally occurring montmorillonite clay contains various metal ions as impurities, typically, titanium and iron. Table 1 lists the components found in sodium montmorillonite mined from Wyoming (WY-MMT), calcium montmorillonite mined from Texas (TX-MMT), and Laponite®. Laponite® is an entirely synthetic layered silicate resembling in both structure and composition the natural smectite mineral hectorite. The sodium montmorillonite from Wyoming (hereafter WY-MMT), designated as Na<sup>+</sup>MMT in the previous paper [1], possesses small amounts of titanium and iron while the synthetic clay, Laponite®, contains insignificant amounts of metal. The TX-MMT, a type of calcium montmorillonite, is a special and somewhat rare clay material that is white in color because of its lower iron content [19,20]. It is especially attractive for this study because it has lower content of iron, a possible source of color formation, than WY-MMT. The presence of titanium or iron could lead to color formation by reaction with phenolic end groups in the degraded polycarbonates. In addition to the metal in the clays, the surface charge of the platelets may play some role in promoting thermal degradation.

## 3. Experimental

### 3.1. Materials

Two commercial polycarbonates having high and medium molecular weight, i.e. HMW and MMW-PC described in the previous paper were used to form the melt compounded composites discussed here [1]. In addition to the organoclays based on WY-MMT described in Table 2 of the previous paper [1], the current paper considers a natural TX-MMT and a synthetic hectorite, Laponite® (LP). These clays were exchanged with two surfactants: bis(2-hydroxy-ethyl)methyl tallow, (HE)<sub>2</sub>M<sub>1</sub>T<sub>1</sub>, and bis(2-hydroxy-ethyl)methyl octadecyl ammonium chloride, (HE)<sub>2</sub>M<sub>1</sub>(C<sub>18</sub>)<sub>1</sub>. The level of amine added to the TX-MMT and Laponite® were 80 and 90 milliequivalent ratio. In preparation of organoclays based on TX-MMT, the calcium ions in bentonite were exchanged with sodium ions and subsequently with surfactant. The d-spacings of the organoclays based on the TX-MMT were measured by X-ray diffraction to give 14.7 Å for (HE)<sub>2</sub>M<sub>1</sub>T<sub>1</sub> and 17.3 Å for (HE)<sub>2</sub>M<sub>1</sub>(C<sub>18</sub>)<sub>1</sub>. Pristine Laponite® has a d-spacing of 12.6 Å at 50% relative humidity. However, it was not possible to obtain d-spacing data for the organoclays based on Laponite® since the X-ray scan did not reveal any structural pattern. This may be related to the smaller aspect ratio of the Laponite® platelets leading to the platelet movement and flocculation during organoclay preparation; the platelets can ‘settle in’ to the flocculated state without good order.

### 3.2. Melt processing

Two co-rotating, intermeshing twin screw extruders were used to form polycarbonate nanocomposites: a Haake twin screw extruder (diameter = 30 mm, *L/D* = 10) was used to prepare the majority of the PC nanocomposites, including those discussed in the previous paper [1] while a Werner and Pfleiderer ZSK 25 (diameter = 25 mm, *L/D* = 48) extruder was used to prepare selected samples for comparative purposes. Some extrusion variables were kept constant, i.e. barrel temperature at 260 °C and screw speed at 280 rpm for

Table 1  
Elemental composition of various clays in wt%

Clays	SiO <sub>2</sub>	Al <sub>2</sub> O <sub>3</sub>	Na <sub>2</sub> O	MgO	Fe <sub>2</sub> O <sub>3</sub>	TiO <sub>2</sub>	LOI <sup>a</sup>	Residual <sup>b</sup>
WY-MMT <sup>c</sup>	55.9	19.2	3.8	2.1	4.3	0.1	14.3	0.3
TX-MMT <sup>d</sup>	65.2	14.5	4.1 <sup>a</sup>	3.4	1.0	0.2	10.7	0.9
Laponite <sup>®e</sup>	48.9	<0.03	5.0	25.4	<0.04	0.01	20.3	0.3

<sup>a</sup> Loss on ignition values reflect all organic species and all volatiles including moisture.

<sup>b</sup> Residual contains ppm of K<sub>2</sub>O, CaO, P<sub>2</sub>O<sub>5</sub>, MnO, Cr<sub>2</sub>O<sub>3</sub>, Ba, Ni, Sr, Zr, and, etc.

<sup>c</sup> Sodium montmorillonite from Wyoming, USA, a higher iron content mineral.

<sup>d</sup> Calcium montmorillonite from Texas, USA, a lower iron content mineral. Calcium ions were exchanged with sodium ions before elemental analysis.

<sup>e</sup> Laponite® is a synthetic hectorite without iron. Laponite® is a registered trademark of Rockwood Specialties, Inc.

Table 2

Measured mechanical properties for the nanocomposites prepared using the ZSK 25 twin screw extruder

Clay	MMT%	Modulus (GPa)	Yield strength (MPa)	Elongation at break (%) <sup>a</sup>
HMW-PC/(HE) <sub>2</sub> M <sub>1</sub> T <sub>1</sub>	2.4	2.82	67.0	109.4
	<b>4.5</b>	<b>3.35</b>	<b>71.5</b>	<b>16.0</b>
HMW-PC/M <sub>1</sub> (HT) <sub>2</sub>	2.3	2.65	63.0	99.4
	<b>4.1</b>	<b>3.06</b>	<b>65.2</b>	<b>60.5</b>
HMW-PC/M <sub>2</sub> (HT) <sub>2</sub>	2.4	2.59	61.7	82.4
	<b>4.5</b>	<b>2.99</b>	<b>63.3</b>	<b>13.4</b>
HMW-PC/WY-MMT	2.4	2.40	59.9	106.5
	<b>4.5</b>	<b>2.61</b>	<b>60.7</b>	<b>49.7</b>
MMW-PC/(HE) <sub>2</sub> M <sub>1</sub> T	2.6	2.85	67.2	91.7
	<b>4.7</b>	<b>3.34</b>	<b>(63.4)</b>	<b>3.0</b>

<sup>a</sup> Crosshead speed = 5.1 cm/min.

both extruders; however, the feed rates were 980 g/h for a the Haake and 4.9 kg/h for the ZSK 25 extruders.

### 3.3. UV–Vis spectroscopy

To gain insights about thermal degradation and color formation of the PC nanocomposites, UV–Vis spectra were obtained using the following two different techniques.

**Solution spectra.** Polycarbonate nanocomposite samples were dissolved in HPLC grade tetrahydrofuran (THF) or chloroform to give solutions in the 10<sup>−3</sup> M range based on the gram molecular weight of the PC repeat unit of 254. The absorbances at 287 nm (phenolic groups) and 265 nm (ester groups) were measured using a Varian Cary IE UV–Vis spectrophotometer in the automatic baseline-correction mode. The spectra were normalized for solution concentration. The ratio, *R*, of the absorbances at 287 nm (phenolic) and 265 nm (ester) was calculated.

**Film spectra.** From a 1 wt% solution in chloroform, thin films of the extruded nanocomposites were cast on a quartz disk by a spin caster at 2000 rpm. The thickness was controlled to be about 1–2 μm. Baseline correction was made with a quartz disk and then the spectra were obtained using a HP 845X UV–Vis spectrometer. Comparison films were cast on silicon wafers using identical conditions in order to measure thickness using an Alpha-step 200, Tenor Instrument. The spectra were normalized using this film thickness.

### 3.4. Color measurement

Color values of injection molded PC nanocomposite bars were determined in the reflective mode by a colorimeter, MICRO S-5 Brightmeter equipped with a quartz–tungsten–halogen lamp. The chromaticity coordinates, *L*<sup>\*</sup>, *a*<sup>\*</sup>, *b*<sup>\*</sup>, were computed using a series of formulae described in ASTM E313. The CIELAB tristimulus color value, *L*<sup>\*</sup>, represents the darkness of color in the chromaticity coordinates, which can be obtained by CIE tristimulus red, green, and blue responses [21].

The yellowness index (YI) was calculated from transmittance values from the solid-state UV–Vis spectra, obtained by the HP 845X UV–Vis spectrometer, using Izod bars and Gardner disks. Then, YI was calculated using the following relationship [22]:

$$YI = \frac{T_{680} - T_{420}}{T_{560}} \quad (1)$$

where *T* is the transmittance at the selected wavelength.

### 3.5. Wide angle X-ray diffraction (WAXD)

WAXD was conducted using a Sintag XDS 2000 diffractometer. WAXD scans were obtained in reflection mode using an incident X-ray wavelength of 1.542 Å at a scan rate of 1.0 deg/min. X-ray analysis was performed on Izod bars except for the organoclay itself, which was in powder form.

### 3.6. Rheology

Dynamic rheological measurements were performed using a Rheometrics rotational rheometer (ARES). Rheological properties of the virgin polycarbonate and the nanocomposites based on various organoclays were measured using 25 mm diameter parallel plates in oscillatory shear mode. Dynamic storage modulus, *G*<sup>′</sup>, and dynamic loss modulus, *G*<sup>″</sup>, were recorded as functions of angular frequency, *ω*, at 260 °C. The frequency sweep was done in the range from 0.01 to 100 rad/s. A fixed strain of 0.1 was used to ensure that measurements were taken within the linear viscoelastic range of the materials. Test specimens were taken from tensile bars, which were dried for 16 h in a vacuum oven at 80 °C prior to each experiment. Experiments were conducted under a nitrogen atmosphere in order to minimize oxidative degradation of the specimens during testing.

#### 4. Effects of extruder type on nanocomposite mechanical properties

The extruder type and screw configuration affects the mean residence time, residence time distribution, and shear history of the product. The Haake co-rotating intermeshing extruder consists of two kneading blocks as described in a prior paper [23]. The ZSK-25 co-rotating extruder consists of three kneading blocks located at 300, 550, and 860 mm, respectively, from the hopper. The first and second kneading disk blocks consist of one left-handed plus five right-handed and two left-handed plus two right-handed kneading disks, respectively. The third kneading block consists of three medium pitch right-handed kneading disks. This configuration is designed to give higher shear intensity produced by a tighter clearance between the barrel and the mixing elements.

Fig. 1 shows the residence time distribution determined by adding 5 g of WY-MMT to the hopper and then measuring ash content of collected samples of polycarbonate extrudate after passing through the twin screw extruder. In past studies, aluminum beads were used to determine the residence time distribution [23,24]; in this study, however, the large diameter ( $D = 1\text{--}2\text{ mm}$ ) and hardness of the aluminum flakes caused a decrease in screw speed while feeding these materials to the ZSK 25 extruder. The Haake extruder shows a mean residence time, 199 s, similar to that found using aluminum flakes in nylon 6 while the ZSK 25 extruder gives 122 s, shorter than that the Haake extruder. The ZSK 25 also has a more narrow distribution of residence times. The latter is related to the tight clearances (0.2–0.3 mm) in the ZSK 25 extruder which provides better

self-wiping effects. The shorter mean residence time and the wider residence time distribution in the Haake extruder is related to its larger clearances (0.5 mm). The backmixing is more dominant in the Haake extruder since the lower  $L/D$  should lead to a shorter residence time. The feed rate to the ZSK extruder was approximately five times greater than the feed rate to the Haake. Other things being equal, a higher feed rate shortens the mean residence time [25]. However, one must also consider the difference in free volume per unit length or potential capacity, i.e. the difference in  $L/D$  for the two extruders. The two feed rates are approximately the same when normalized by  $L/D$ . The volumetric feed rate does affect the filling factor in the channel, which in turn affects the residence time, and the level of shear.

The effects of extruder type on the dispersion of the organoclay in polycarbonate was explored using three organoclays based on WY-MMT exchanged with  $M_2(HT)_2$ ,  $M_1H_1(HT)_2$ , and  $(HE)_2M_2T_1$ . Mechanical properties were measured for two target MMT loadings, 2.4 and 4.5 wt%, using HMW-PC as the matrix. The resulting MMT contents and mechanical properties are listed in Table 2. For direct comparisons, the data were interpolated or extrapolated to the target loadings, as described in the previous paper [2]; these results are summarized in Table 3.

Fig. 2 compares the mechanical properties of the PC nanocomposites prepared using the Haake and ZSK 25 twin screw extruders. The nanocomposites prepared by the Haake extruder tend to have a higher moduli than those formed by the ZSK 25 extruder as seen in Fig. 2(a). As described earlier, the screw configuration of the Haake extruder may be considered to produce a medium shear intensity while the screw configuration of the ZSK-25 extruder is designed to produce a high shear intensity. One might expect the high shear intensity screw to be more efficient for exfoliation of the aluminosilicate layers. However, in a prior paper which used a wide range of twin screw extruders and screw configurations, it was found that the level of aluminosilicate exfoliation depends on the residence time as well as residence time distribution and is not always improved by higher intensity of shear [26]. Fig. 2(b) shows that the yield strength is more or less the same for nanocomposites produced by the Haake and the ZSK 25 extruders. The elongation at break, see Fig. 2(c), does not show a well defined trend according to extruder type; however, one might consider that nanocomposites formed in the ZSK 25 tend to have better elongation at break in some cases. The above trends are consistent with somewhat better dispersion of the organoclays in the PC matrix for the Haake than the ZSK 25.

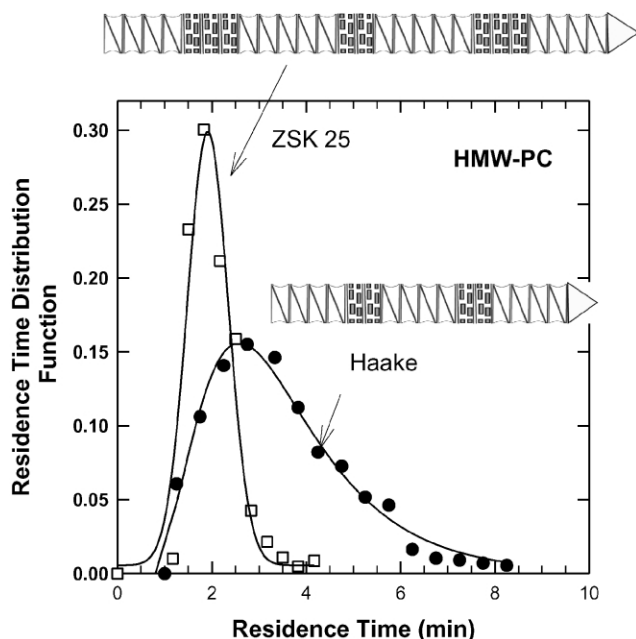


Fig. 1. Residence time distribution curves for the Haake (●) and ZSK 25 (□) twin screw extruders at the die exit for HMW polycarbonate. Schematic screw configurations are included.

#### 5. Effects of organoclay type on color formation

Fig. 3 shows the color of HMW-PC nanocomposites, containing 2.4% MMT loading, formed from various organoclays in both visual and quantitative ways. Fig. 3(a)

Table 3  
Mechanical property data interpolated or extrapolated to the targeted MMT loading levels

PC/organoclay	Nanocomposite (wt% MMT)	Modulus (GPa)	Yield strength (MPa)	Elongation at break (%)
HMW-PC/(HE) <sub>2</sub> M <sub>1</sub> T <sub>1</sub>	2.4	2.82	67.0	109.4
	4.5	3.35	71.5	16.0
HMW-PC/M <sub>1</sub> H <sub>1</sub> (HT) <sub>2</sub>	2.4	2.67	63.1	97.5
	4.5	3.08	65.3	58.6
HMW-PC/M <sub>2</sub> (HT) <sub>2</sub>	2.4	2.59	61.7	82.4
	4.5	2.99	63.3	13.4
HMW-PC/WY-MMT	2.4	2.40	59.9	106.5
	4.5	2.61	60.7	49.7
MMW-PC/(HE) <sub>2</sub> M <sub>1</sub> T <sub>1</sub>	2.4	2.85	67.2	91.7
	4.5	3.34	–	2.95

compares the color of nanocomposites prepared from various organoclays using the Haake twin screw extruder. In general, the depth of color determined visually shows a good correlation with the  $L^*$  value. However, the yellowness index obtained from transmittance data do not show as good a correlation with the color depth. This yellowness index was briefly used by ASTM but was eventually replaced by CIE tristimulus color values [27]. It is interesting to see that the composites from WY-MMT show the dark color even though the clay particles were poorly dispersed; high dispersion leads to more exfoliation of clay surface to PC and then a greater opportunity for clay-induced chemical reactions. The nanocomposite formed from the surfactant substituted by benzyl and hydrogenated tallow, M<sub>2</sub>B<sub>1</sub>(HT)<sub>1</sub>, gives the lightest color while the one formed from the surfactant substituted by hydroxy-ethyl and tallow, (HE)<sub>2</sub>M<sub>1</sub>T<sub>1</sub>, gives the darkest color. In a series of quaternary ammonium surfactants, the hydrogenated tallow substituted organoclays show lighter color than the tallow substituted ones. The tallow tails in organoclays contain double bonds, approximately 48.3% chains with one or two double bonds, which at elevated temperature may produce free radicals by thermal or oxidation mechanisms that in turn can react with polycarbonate [2]. Organoclays based on tertiary amines having either one or two hydrogenated tallow tails lead to darker color than the corresponding quaternary amines, i.e. M<sub>2</sub>H<sub>1</sub>(HT)<sub>1</sub> and M<sub>1</sub>H<sub>1</sub>(HT)<sub>2</sub> versus M<sub>3</sub>(HT)<sub>1</sub> and M<sub>2</sub>(HT)<sub>2</sub>, even though the levels of dispersion are comparable. The difference in color may be related to differences in stability of tertiary amine versus quaternary amine surfactants.

Fig. 3(b) shows color comparisons for nanocomposites prepared by the Haake versus the ZSK 25 twin extruders for three selected organoclays, M<sub>2</sub>(HT)<sub>2</sub>, M<sub>1</sub>H<sub>1</sub>(HT)<sub>2</sub>, and (HE)<sub>2</sub>M<sub>1</sub>T<sub>1</sub>. Overall, the Haake extruder leads to darker colors for the nanocomposites than the ZSK 25 extruder. This color difference may be related to the residence time of polycarbonate in the extruder; the materials experienced longer time at elevated temperature in the Haake. In addition, the broader residence time distribution for the Haake extruder means some portion of the extruded material experienced considerably longer time in the extruder than the mean residence time.

One might anticipate that exposing more clay surface area to PC would lead to a greater extent of color formation since this would give more opportunity for chemical reactions induced by the organoclay to occur. Certainly better dispersion of the clay leads to a greater degree of reinforcement [24,28]. Based on these premises, there might be a trade-off relationship between mechanical properties and the depth of color for PC nanocomposites. To explore this, plots of modulus are shown in Fig. 4 versus the quantitative measures of color given in Fig. 3; Fig. 4(a) shows modulus versus the yellowness index while Fig. 4(b) shows modulus versus  $L^*$ . Note that the color data in Fig. 3 were measured using injection-molded bars having thickness of 3.175 mm. Fig. 4(a) and (b) suggest no discernable correlation between color index and modulus. This implies that color formation involves other factors than simply how much clay surface area is in contact with the PC matrix. However, the nanocomposites formed from selected organoclays using the ZSK-25 extruder do show a good correlation between modulus and yellowness index using the data from Fig. 3(b). The data in parenthesis were measured using injection-molded Gardner disks with thickness about 1 mm. For this limited set of samples, there seems to be a relationship between the degree of dispersion of clay in the PC matrix as indicated by modulus and extent of color formation, see Fig. 4(c). As expected, the yellowness index is dependent on the thickness of the sample; thicker samples give higher values of the yellowness index.

UV–Vis spectroscopy was employed to seek clues about the nature of the chromophores that give such deep colors in the PC nanocomposites. Fig. 5(a) shows the spectra in the UV and visible regions for THF solutions obtained from nanocomposites, containing 2.4% of MMT, formed from various organoclays. The visible region does not show any distinct peak that might be indicative of a specific chromophore. Spectra of chloroform solutions also do not show any peak in the visible region. However, there are distinctive peaks in the UV region as seen in Fig. 5(b); the absorbance peaks at 285 and 265 nm have been assigned to phenolic units and the ester moiety of the carbonate groups, respectively [29].

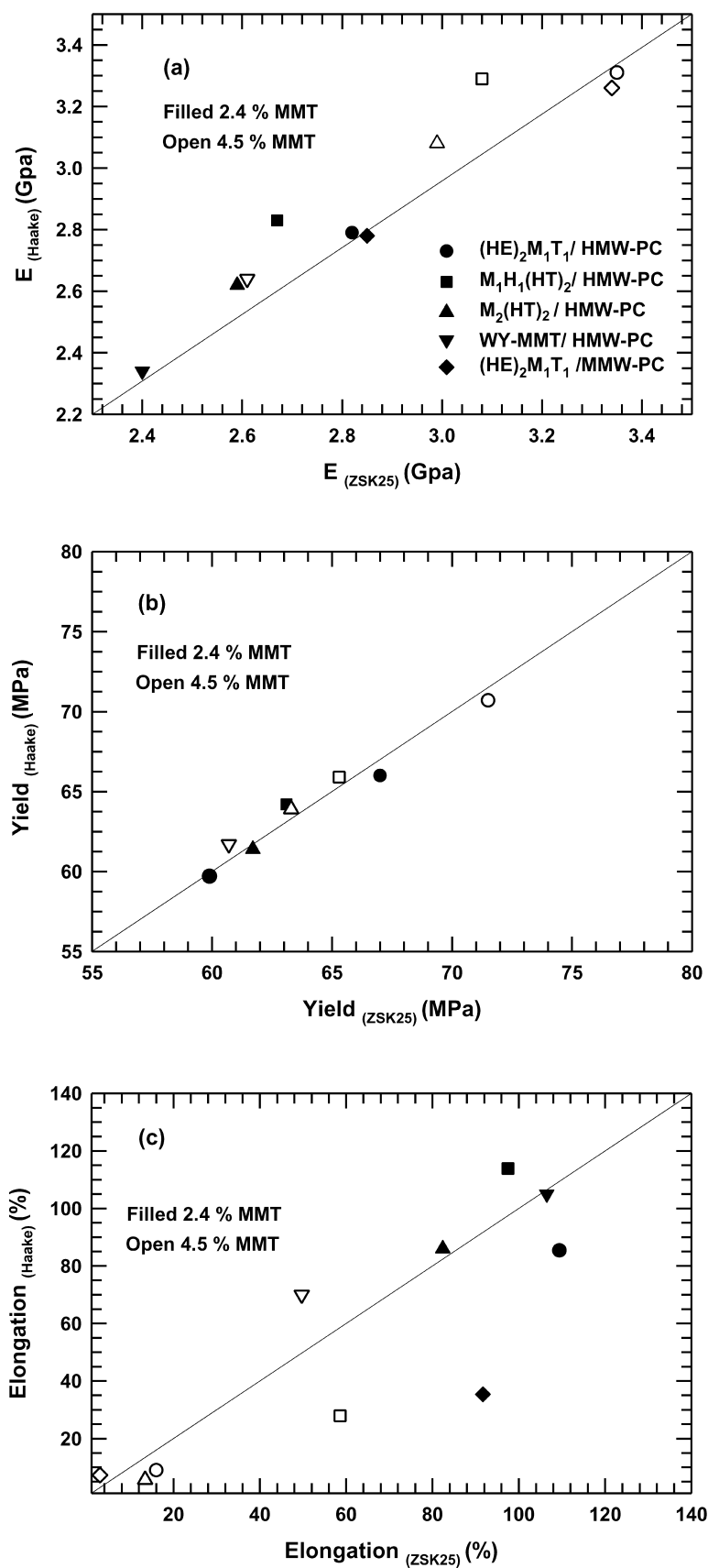


Fig. 2. Comparison of tensile properties of HMW-PC nanocomposites formed from various organoclays made by melt processing using Haake and ZSK 25 twin screw extruders at the MMT content of 2.4% (open points) and 4.5% (filled points): (a) Young's modulus, (b) yield strength, and (c) elongation at break.



(a) Haake Twin Extruder

Organoclays	Appearance	YI	L*	Modulus
HMW-PC		0.053	87	2.15
M <sub>2</sub> B <sub>1</sub> (HT) <sub>1</sub>		1.73	45	2.77
M <sub>2</sub> (HT) <sub>2</sub>		2.40	47	2.62
M <sub>3</sub> (HT) <sub>1</sub>		2.28	39	2.65
(EO <sub>m</sub> ) <sub>1</sub> (EO <sub>n</sub> ) <sub>1</sub> M <sub>1</sub> (C <sub>18</sub> ) <sub>1</sub>		4.04	39	2.90
WY-MMT		3.54	23	2.34
M <sub>1</sub> H <sub>1</sub> (HT) <sub>2</sub>		2.06	21	2.83
M <sub>2</sub> H <sub>1</sub> (HT) <sub>1</sub>		2.48	15	2.70
M <sub>3</sub> T <sub>1</sub>		3.31	10	2.65
H <sub>3</sub> (12-ALA) <sub>1</sub>		-	6	2.48
(HE) <sub>2</sub> M <sub>1</sub> T <sub>1</sub>		6.75	3	2.81

(b) Color comparison of nanocomposites prepared using Haake and ZSK 25 extruders

Organoclays	Appearance	YI	L*	Modulus
M <sub>2</sub> (HT) <sub>2</sub> -Haake		2.40	47	2.62
M <sub>2</sub> (HT) <sub>2</sub> -ZSK25		2.30 (1.13)	50	2.59
M <sub>1</sub> H <sub>1</sub> (HT) <sub>2</sub> -Haake		2.06	21	2.83
M <sub>1</sub> H <sub>1</sub> (HT) <sub>2</sub> -ZSK25		1.75 (1.07)	40	2.65
(HE) <sub>2</sub> M <sub>1</sub> T <sub>1</sub> -Haake		6.75	3	2.79
(HE) <sub>2</sub> M <sub>1</sub> T <sub>1</sub> -ZSK25		2.92 (1.32)	24	2.82

Fig. 3. Effect of organoclay type on color appearance of HMW-PC nanocomposites made by melt processing using (a) Haake and (b) ZSK 25 twin screw extruders and corresponding yellow index and  $L^*$  value. YI and  $L^*$  were measured using injection-molded bars (thickness = 0.32 cm) of 2.4 wt% MMT while data in parenthesis were measured using Gardner disks (thickness = 0.1 cm).

To better see the phenolic region of the spectra, enlarged plots of the wavelength range from 260 to 300 nm are shown in Fig. 6. Fig. 6(a) shows that the pure HMW-PC has a very low concentration of phenolic end groups while the nanocomposites formed from it have higher levels of phenolic groups that depend on the organoclay used. A more clear representation can be made by normalizing the spectra by the maximum absorbance at 265 nm and then subtracting the pure HMW-PC spectrum as shown in Fig. 6(b). Fig. 6 suggests that the polycarbonate molecules in the nanocomposite have undergone chain scission by a mechanism that leads to phenolic ends. The nanocomposites

formed from organoclays containing hydroxy-ethyl and tallow groups show higher concentrations of phenolic groups than those containing hydrogenated tallow units. This molecular weight degradation of polycarbonate can be seen more directly from intrinsic viscosity measurements before and after melt compounding. Molecular weights calculated from the intrinsic viscosity using the Mark–Houwink equation [30] are shown in Table 4 for nanocomposites formed from the organoclay based on (HE)<sub>2</sub>M<sub>1</sub>T<sub>1</sub>; a molecular weight reduction of about 33% was observed when the matrix was HMW-PC while the molecular weight reduction was about 18% when the matrix was LMW-PC. As described earlier, the nanocomposite based on HMW-PC gives a larger extent of modulus enhancement which reflects greater exfoliation of organoclay particles. The greater molecular weight reduction in this case may be the result of greater exposure of polycarbonate to the platelet surface that causes chain scission as argued earlier.

Shchori and McGrath developed a UV analysis method in THF solution to monitor molecular weight during polymerization of uncapped PC samples having low molecular weight [29]. They used the ratio of the absorbances at 287 and 265 nm,  $R^*$ , to calculate  $\bar{M}_n$  based on the premise that  $R(= 1/R^*)$  reflects the number of repeat units per OH end group if the molar extinction coefficient is known. They calculated the number-average molecular weight,  $\bar{M}_n$ , using the following expression:

$$\bar{M}_n = \frac{3450}{R^* \times 4.29 / (1 - 0.17R^*) - 0.03} \quad (2)$$

where they took the extinction coefficient of ester groups at 287 nm to be 3450 and the absorptivities of a capped polycarbonate at 287 and 265 nm to be 4.29 and 0.03, respectively. Below we will discuss  $R$  values determined in THF solutions for the PC nanocomposites and their corresponding number average molecular weights calculated using Eq. (2).

Table 5 gives the  $R$  values and their corresponding  $\bar{M}_n$  for the nanocomposites prepared by both extruders. The  $R$  value for the pure HMW-PC is high and is comparable to that reported for capped polycarbonate [29]; however, the  $\bar{M}_n$  calculated from  $R$  for pure HMW-PC, 27,800 g/mol, is much higher than that determined using GPC, 10,800 g/mol [30,31]. The  $R$  values for the nanocomposites in this study

Table 4  
Intrinsic viscosity of polycarbonate nanocomposites

	Intrinsic viscosity (100 ml/g)	$\bar{M}_n$ (g/mol) <sup>a</sup>
HMW-PC pure	0.62	30,000
HMW-PC/(HE) <sub>2</sub> M <sub>1</sub> T <sub>1</sub> -3.3% MMT	0.46	20,000
MMW-PC pure	0.49	22,000
MMW-PC/(HE) <sub>2</sub> M <sub>1</sub> T <sub>1</sub> -3.4% MMT	0.37	18,000

<sup>a</sup>  $[\eta] = 3.01 \times 10^{-4} \bar{M}_n^{0.74}$  [30].

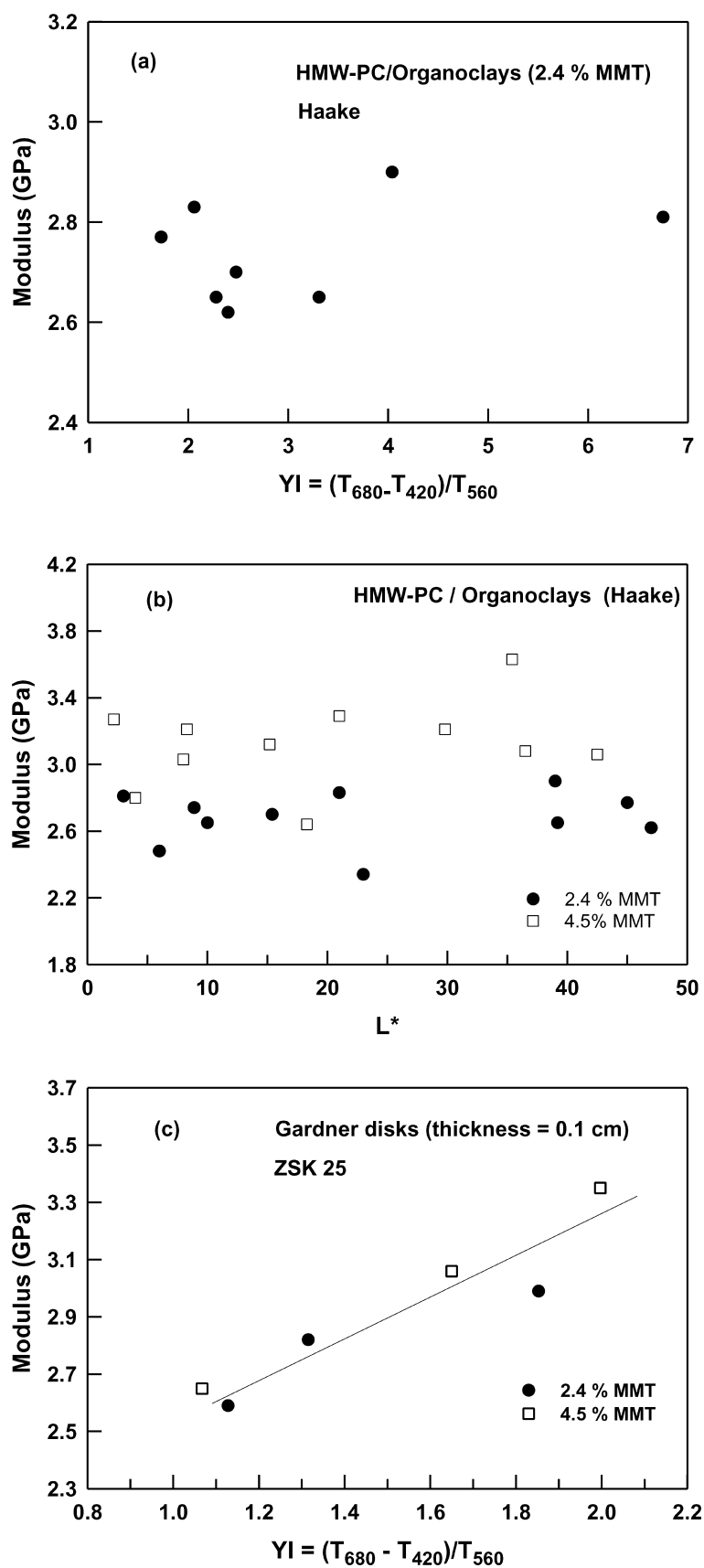


Fig. 4. Relationships between (a) modulus and yellowness index, (b) modulus and  $L^*$  measured from tensile bars, and (c) modulus and yellowness index measured from disks.



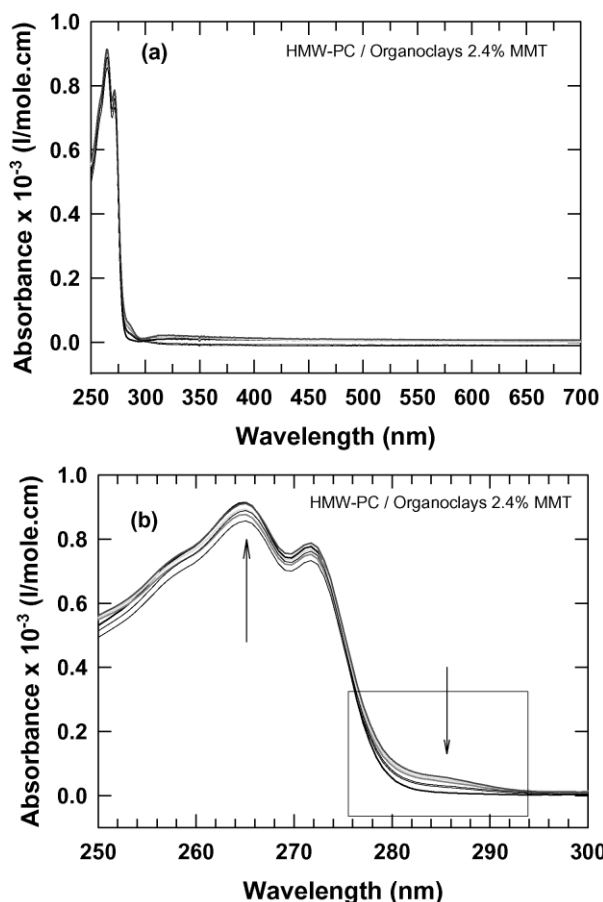


Fig. 5. UV-Vis spectra of THF solutions of HMW-PC nanocomposites in the range of (a) 250–700 nm and (b) 250–300 nm. Arrows indicate the absorbance peaks at 265 nm from ester groups and at 287 nm from phenolic groups.

were found to be much lower than that of pure HMW-PC which is indicative of a molecular weight degradation process leading to phenolic end groups. The  $R$  values measured for thin films are also listed in Table 5; the solid state measurements give lower  $R$  values than those in solution. It is also useful to note that the Haake extruder produces nanocomposites with lower  $R$  values or higher phenolic group contents than the ZSK 25 extruder. For the PC nanocomposites, several trends can be drawn from Table 5: (1) saturated tails lead to higher  $R$  value, (2) two tails lead to higher  $R$  value, and (3) hydroxy-ethyl groups lead to lower  $R$  value (higher reduction of molecular weight) regardless of tail type.

Based on the work of Smith et al. [18] we might expect a relationship between the number of phenolic end-groups and the extent of color formation in the PC nanocomposites as discussed earlier. Fig. 7(a) shows a plot of  $L^*$  versus the corresponding  $R$  value for the nanocomposites prepared using the Haake extruder. There is no unique trend between these two parameters; this suggests that the mechanism of color formation cannot be simply explained only in terms of only the phenolic end-group content in the nanocomposites. However, there does seem to be a good correlation of

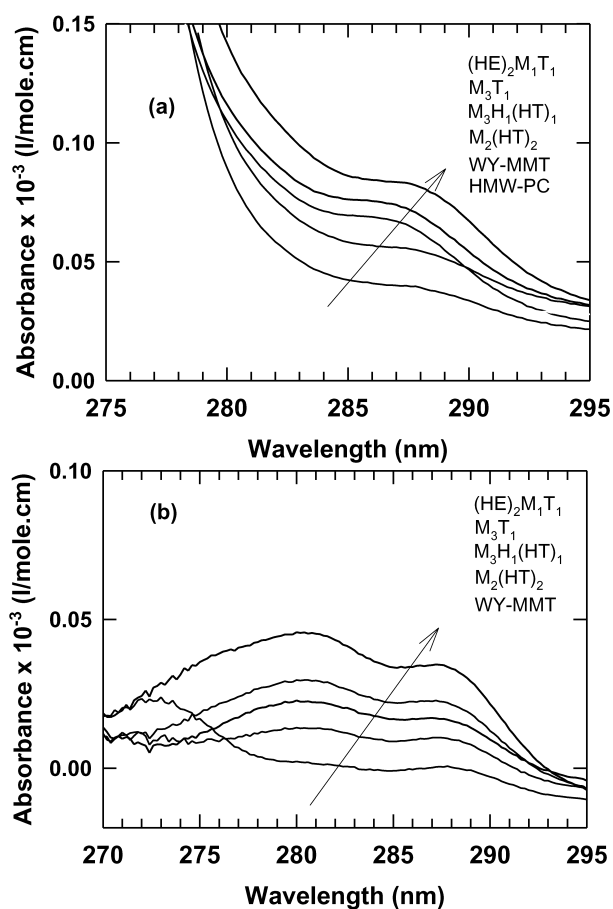


Fig. 6. (a) Absorbance of phenolic region for HMW-PC nanocomposite solutions and (b) absorbance of phenolic region for HMW-PC nanocomposite solutions subtracted by the absorbance of pure polycarbonate solution.

nanocomposite modulus with the corresponding  $R$  value as seen in Fig. 7(b). This result implies that the molecular weight of the PC matrix decreases as the modulus increases in these PC nanocomposites. There is good evidence to show that enhancement in stiffness reflects the level of exfoliation in the matrix. Of course, the better dispersion of the organoclay, the more of its surface area is exposed to the PC matrix, and it seems that this enhances the extent of degradation of the polycarbonate. The above evidence suggests that the chemical processes that lead to molecular weight degradation and to color formation are not uniquely connected.

## 6. Rheological behavior

Recent studies have shown that the dynamic properties of polymers containing nanofillers [24,32–35] have the same general characteristics as conventional filled materials: failure of Cox–Merz rule [24], solid-like behavior at lower frequency [24,32–34], and percolation above a certain particle concentration [35]. However, the interesting observation is that nanofillers show such behaviors at much

Table 5

*R* values determined in THF solution for HMW-PC/organoclay nanocomposites prepared using the Haake and the ZSK-25 extruders

PC/organoclays	Nanocomposites (% MMT)	$R = A_{265}/A_{287}$	$\bar{M}_n$	Extruder type
HMW-PC		27.9 (24.1) <sup>a</sup>	27,800	
Na <sup>+</sup> MMT	2.4	27.3	26,900	Haake
	4.5	18.5	16,900	Haake
(12-ALA) <sub>1</sub> H <sub>3</sub>	2.5	17.2	15,500	Haake
	4.6	12.3	10,700	Haake
M <sub>2</sub> (HT) <sub>2</sub>	2.4	16.0 (11.4)	14,300	Haake
	4.4	7.0	5800	Haake
	4.5	7.8	6500	ZSK25
M <sub>3</sub> (HT) <sub>1</sub>	1.9	15.0	13,300	Haake
	4.4	7.5	6200	Haake
M <sub>2</sub> H <sub>1</sub> (HT) <sub>1</sub>	2.4	14.9	13,200	Haake
	4.5	8.7	7300	Haake
M <sub>1</sub> H <sub>1</sub> (HT) <sub>2</sub>	2.4	17.3	15,700	Haake
	4.5	10.5	12,000	Haake
	4.5	17.3	15,700	ZSK 25
M <sub>2</sub> B <sub>1</sub> (HT) <sub>1</sub>	2.4	13.5	11,800	Haake
	4.5	8.2	6800	Haake
M <sub>3</sub> T <sub>1</sub>	2.4	13.5 (10.8)	11,800	Haake
	4.5	7.7	6400	Haake
(HE) <sub>2</sub> M <sub>1</sub> (C <sub>18</sub> ) <sub>1</sub>	2.4	11.0	9400	Haake
	4.5	7.1	5900	Haake
(HE) <sub>2</sub> M <sub>1</sub> T <sub>1</sub>	2.5	11.5 (8.2)	9900	Haake
	4.4	5.7 (5.6)	4700	Haake
	4.5	7.4	6100	ZSK 25
(EO <sub>m</sub> ) <sub>1</sub> (EO <sub>n</sub> ) <sub>1</sub> M <sub>1</sub> (C <sub>18</sub> ) <sub>1</sub>	2.4	9.7	8200	Haake
	4.6	6.3	5200	Haake

<sup>a</sup> Data in parenthesis measured using thin films (1–2 μm).

lower concentrations than conventional fillers [36,37]. Since the rheological properties are functions of both the morphological state of the filler and the molecular weight of the matrix, such measurements can, to some extent, be used to monitor both issues [38]. In a recent paper, the degradation of nylon 6 matrix was suggested from the observation that the nanocomposite had a lower viscosity than the neat nylon 6 [24].

Fig. 8 shows the dynamic rheological properties of nanocomposites, containing 4.5 wt% MMT, formed from selected organoclays, M<sub>3</sub>T<sub>1</sub>, M<sub>2</sub>(HT)<sub>2</sub>, (HE)<sub>2</sub>M<sub>1</sub>T<sub>1</sub>, and (EO<sub>m</sub>)<sub>1</sub>(EO<sub>n</sub>)<sub>1</sub>M<sub>1</sub>(C<sub>18</sub>)<sub>1</sub> with HMW-PC. The data for the composites formed from WY-MMT and pure HMW-PC are also included in the plots. The storage modulus ( $G'$ ) of nanocomposites shows higher values at low frequencies than pure HMW-PC but lower values at high frequencies as seen Fig. 8(a). Solid-like behavior, i.e. the slope of  $\log G'$  versus  $\log \omega$  is less than 2, is observed over the entire region of frequencies for the nanocomposites. A similar result was reported for nylon 6 nanocomposites [24]. It is interesting to see that the storage modulus at a low frequency, e.g. 0.1 rad/s, varies with the structure of the organoclays in the following order: M<sub>2</sub>(HT)<sub>2</sub> > (EO<sub>m</sub>)<sub>1</sub>(EO<sub>n</sub>)<sub>1</sub>M<sub>1</sub>(C<sub>18</sub>)<sub>1</sub> > M<sub>3</sub>T<sub>1</sub> > (HE)<sub>2</sub>M<sub>1</sub>T<sub>1</sub> > WY-MMT > HMW-PC. Since the storage modulus is sensitive to the changes in the morphological state and to the molecular weight of the matrix, the responses of  $G'$  in these materials may reflect at least two different sources: the

level of exfoliation and the molecular weight of the matrix. The solid state moduli for these materials, as reported in the previous paper, stand in the order: (EO<sub>m</sub>)<sub>1</sub>(EO<sub>n</sub>)<sub>1</sub>M<sub>1</sub>(C<sub>18</sub>)<sub>1</sub> > (HE)<sub>2</sub>M<sub>1</sub>T<sub>1</sub> > M<sub>2</sub>(HT)<sub>2</sub> > M<sub>3</sub>T<sub>1</sub> > WY-MMT > HMW-PC. Since solid state stiffness enhancement results from the level of dispersion of the clay, then it seems clear that the trend in  $G'$  for the molten state primarily reflects the morphology of the sample. The two orders of magnitude difference may reflect the molecular weight degradation; less degradation occurred in the M<sub>2</sub>(HT)<sub>2</sub> based nanocomposite while more degradation occurred in the (HE)<sub>2</sub>M<sub>1</sub>T<sub>1</sub> based nanocomposite. These results are consistent with the  $R$  value and color richness. At present, however, it is difficult to offer an explanation for these behaviors due to the lack of explicit details of the morphological states and molecular weight.

Similar trends in loss modulus ( $G''$ ), see Fig. 8(b), are also apparent but are somewhat less pronounced. The terminal slopes at low frequency for pure HMW-PC and the composite formed from WY-MMT are unity while the other nanocomposites show lower slopes. These trends can be seen more clearly in Han plots, i.e. logarithmic plots of  $G'$  versus  $G''$ , in Fig. 8(c). The slope of  $\log G'$  versus  $\log G''$  for HMW-PC is close to 2 as predicted for a homogenous polymer melt [39]. The data for the composites are located above the line of HMW-PC which results from the mixing with stiff clay particles. The nanocomposites formed from M<sub>2</sub>(HT)<sub>2</sub>, (EO<sub>m</sub>)<sub>1</sub>(EO<sub>n</sub>)<sub>1</sub>M<sub>1</sub>(C<sub>18</sub>)<sub>1</sub>, M<sub>3</sub>T<sub>1</sub>, and (HE)<sub>2</sub>M<sub>1</sub>T<sub>1</sub>,

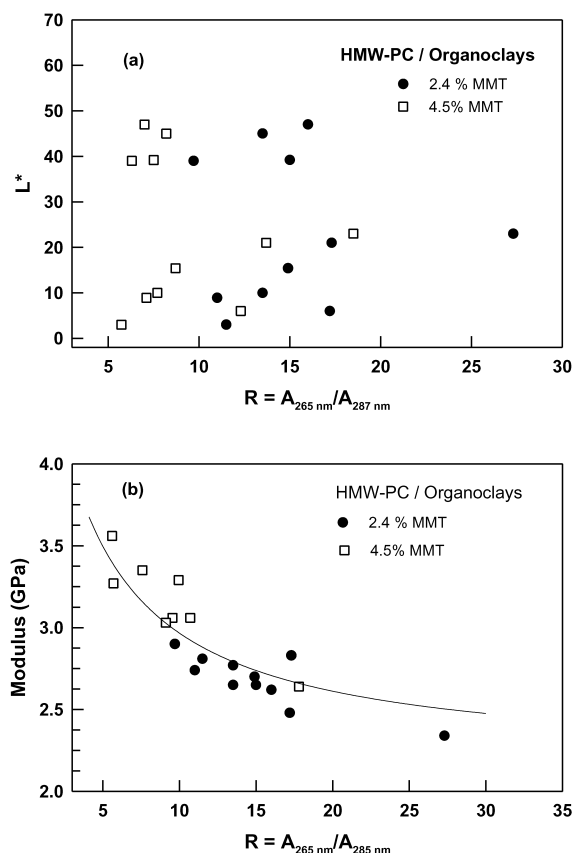


Fig. 7. Relationships between (a)  $L^*$  and  $R$  values and (b) modulus and  $R$  values for HMW-PC nanocomposites formed from various organoclays.

as seen in Fig. 8(a), give very similar viscoelastic behavior at elevated temperature; they deviate from Newtonian behavior over the whole frequency region while the WY-MMT based composite shows very similar behavior as the pure HMW-PC except in the terminal region. The complex viscosities, Fig. 8(d), show non-Newtonian behavior for the nanocomposites formed from organoclays even at the lowest frequencies while Newtonian behavior is observed for the HMW-PC and the composite with WY-MMT. Similar trends are also observed in the levels of the complex viscosity at low frequency for the nanocomposites but the WY-MMT based composite shows lower viscosities than HMW-PC. In general, a composite filled with solid particles should have higher viscosity than the corresponding matrix. The lower values of complex viscosity for the WY-MMT based composite reflect severe reduction in the molecular weight of the PC matrix when mixed with WY-MMT.

## 7. Effects of clay type

As discussed earlier, organoclays based on Laponite<sup>®</sup> and TX-MMT may have some advantages for improvement of the color of PC nanocomposites because of lower contents of iron or titanium. Fig. 9 shows color formation for the HMW-PC nanocomposites formed from selected

surfactants,  $(\text{HE})_2\text{M}_1\text{T}_1$  and  $(\text{HE})_2\text{M}_1(\text{C}_{18})_1$ . The nanocomposites based on Laponite<sup>®</sup> have a light yellow color and less color depth while the composite based on TX-MMT gives similar color but less color depth. These observations are clearly reflected by the  $L^*$  values in Fig. 9; TX-MMT shows the highest  $L^*$  and Laponite<sup>®</sup> gives an almost comparable value. As discussed earlier, the nanocomposite based on  $(\text{HE})_2\text{M}_1\text{T}_1$  surfactant/WY-MMT gives the darkest color observed in this study. From these results, we may conclude that lower contents of Fe and/or Ti ions significantly reduce color formation during melt processing. Of course, the  $(\text{HE})_2\text{M}_1(\text{C}_{18})_1$  surfactant gives less color in all three clays than  $(\text{HE})_2\text{M}_1\text{T}_1$  due to differences in double bond contents of the hydrocarbon tail. The  $R$  values determined in the THF solutions for these nanocomposites are similar for the Laponite<sup>®</sup>, TX-MMT, and WY-MMT-based nanocomposites. This may indicate similar levels of thermal degradation during melt processing. It is surprising to see the high moduli for the PC nanocomposites formed from Laponite<sup>®</sup>. Details of morphology and mechanical properties of these materials are given next.

Fig. 10 shows X-ray diffraction patterns for organoclays formed from Laponite<sup>®</sup> and TX-MMT and their corresponding HMW-PC nanocomposites. The organoclays formed from Laponite<sup>®</sup> do not show any distinctive peaks at a slow scanning rate, 0.03 degree/min; this may be the result of a disordered structure of the layers due to flocculation during recovery from the exchange reaction. The organoclays formed from TX-MMT show the following gallery spacings after the exchange reaction, 14.7 and 17.3 Å for TX-MMT- $(\text{HE})_2\text{M}_1\text{T}_1$  and TX-MMT- $(\text{HE})_2\text{M}_1(\text{C}_{18})_1$ , respectively. Even lower MER values, 80 MER, were used for TX-MMT; using results for WY-MMT [2], the d-spacing would be predicted to be about 18 and 19 Å for TX-MMT- $(\text{HE})_2\text{M}_1\text{T}_1$  and TX-MMT- $(\text{HE})_2\text{M}_1(\text{C}_{18})_1$ , respectively. The X-ray patterns for PC nanocomposites formed from Laponite<sup>®</sup> do not show any peak which may be due to lack of a diffraction pattern for Laponite<sup>®</sup> itself rather than reflecting a high degree of exfoliation. An attempt was made to image the morphology of Laponite<sup>®</sup>/PC composites using transmission electron microscopy (TEM); however, this did not reveal any particles. It is reported that characterization of Laponite<sup>®</sup> by TEM is very difficult because of its transparent nature and low stability [40]. Staining with  $\text{RuO}_4$ ,  $\text{OsO}_4$ , etc. might be a useful way to develop contrast; this was not attempted here. TX-MMT based nanocomposites shows similar patterns as the corresponding nanocomposites formed from WY-MMT; a weak shoulder appears at  $2\theta = 2.7^\circ$  (32.7 Å) and tactoid structure is evident at  $2\theta = 6^\circ$  (14.7 Å).

Fig. 11(a) shows the modulus for HMW-PC nanocomposites formed from three different clays with two different surfactants. Laponite<sup>®</sup> leads to a much higher modulus than the other clays. Only one loading was prepared for the Laponite<sup>®</sup>-based organoclay due to the poor melt strength at higher loadings. In general, the unsaturated tallow tail

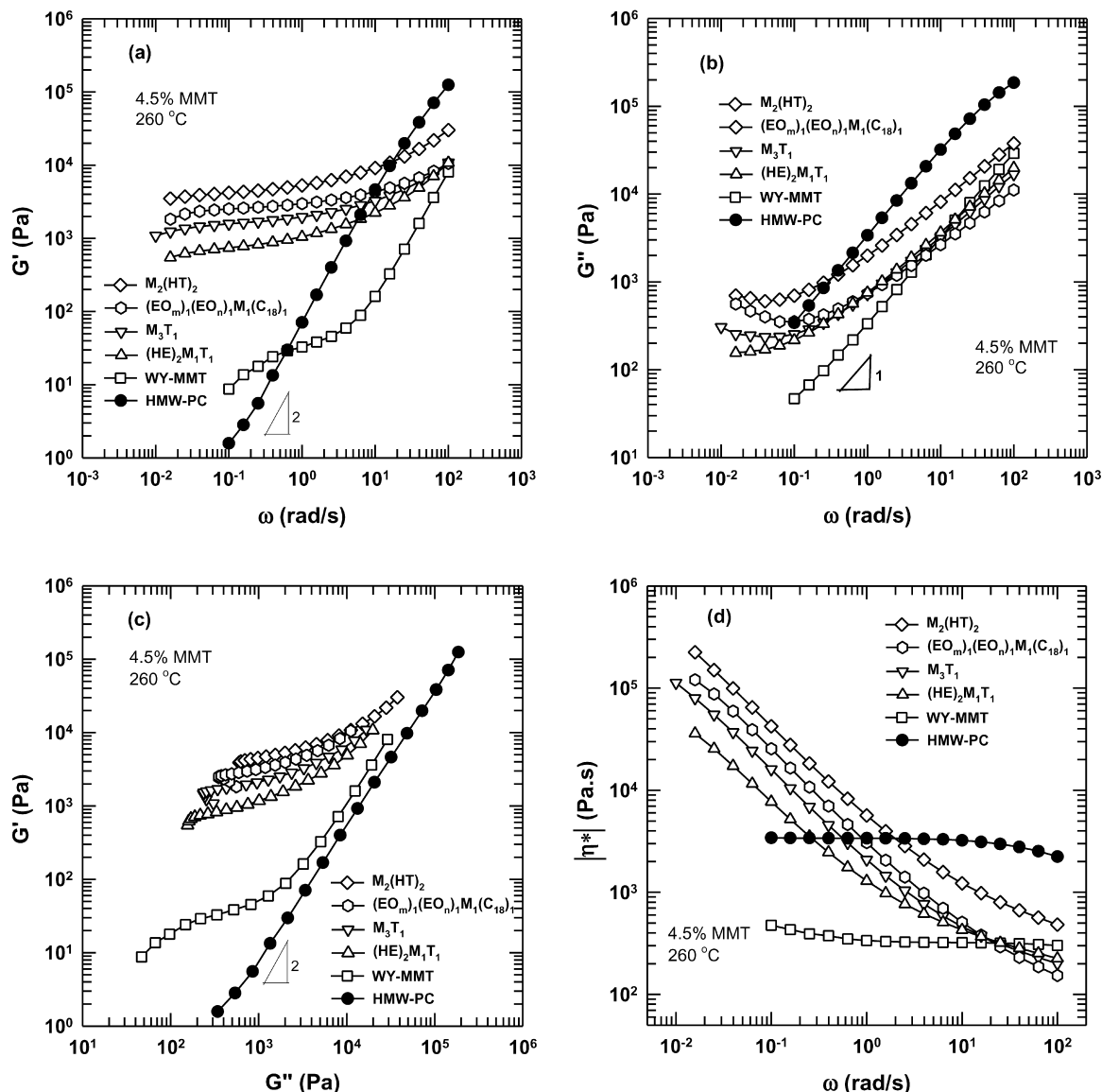


Fig. 8. Dynamic viscoelastic properties as a function of frequency measured from a parallel plate rheometer at 260 °C for pure HMW-PC and its organoclay nanocomposite melts: (a) storage modulus,  $G'$ , (b) loss modulus,  $G''$ , (c)  $\log G'$  versus  $\log G''$ , and (d) complex viscosity. The nanocomposites contain  $\sim 4.5$  wt% MMT.

leads to a higher modulus than does the saturated octadecyl tail. Fig. 11(b) shows elongation at break for the nanocomposites; Laponite<sup>®</sup> based nanocomposites are very brittle even at low loadings while the TX-MMT based nanocomposite shows a better elongation at break but somewhat lower than that for MMT-based nanocomposites at high loadings.

## 8. Conclusions

Polycarbonate nanocomposites were prepared by two different twin screw extruders from a series of organoclays based on WY-MMT exchanged with various amine surfactants. The extruder type and screw configuration

affected the dispersion of the organoclays and in turn color formation. It was found that the extruder with the longer residence time and broader residence time distribution was more effective for dispersing the clay but gave more color.

Visual and quantitative methods were used to show the effect of organoclay structure on color formation during melt processing. A color index determined by colorimeter results shows that the color formation depends on the nature of the surfactant. Double bonds in the surfactant leads to more color depth than saturated surfactants and more severe color was observed in the surfactants containing both hydroxy-ethyl groups and tallow tails. Tertiary amines give darker color than quaternary ammonium surfactants. Selected organoclays from synthetic clay, Laponite<sup>®</sup>, and TX-MMT were also prepared. Laponite<sup>®</sup> and TX-MMT







Organoclays	Appearance	$L^*$	R	Modulus
LP-(HE) <sub>2</sub> M <sub>1</sub> (C <sub>18</sub> ) <sub>1</sub>		40	10.3 (6.5)	2.85
LP-(HE) <sub>2</sub> M <sub>1</sub> T <sub>1</sub>		34	10.4 (6.8)	2.81
TX-MMT-(HE) <sub>2</sub> M <sub>1</sub> (C <sub>18</sub> ) <sub>1</sub>		49	10.1	3.13
TX-MMT-(HE) <sub>2</sub> M <sub>1</sub> T <sub>1</sub>		47	10.1	3.04
WY-MMT-(HE) <sub>2</sub> M <sub>1</sub> (C <sub>18</sub> ) <sub>1</sub>		11	11.0	2.74
WY-MMT-(HE) <sub>2</sub> M <sub>1</sub> T <sub>1</sub>		3	11.5	2.81

Fig. 9. Effect of clay type on color appearance of HMW-PC nanocomposites formed from various organoclays made by melt processing and corresponding  $L^*$ ,  $R$  value, and modulus.  $L^*$  values were measured using injection-molded bars (thickness = 0.32 cm) having 2.4 wt% MMT in the nanocomposites but 4.5 wt% for data in parenthesis.

produce less color formation in PC nanocomposites than montmorillonite due to their lower content of iron ions. The nanocomposites formed from Laponite<sup>®</sup> gives higher modulus than those formed from organoclays based on montmorillonite.

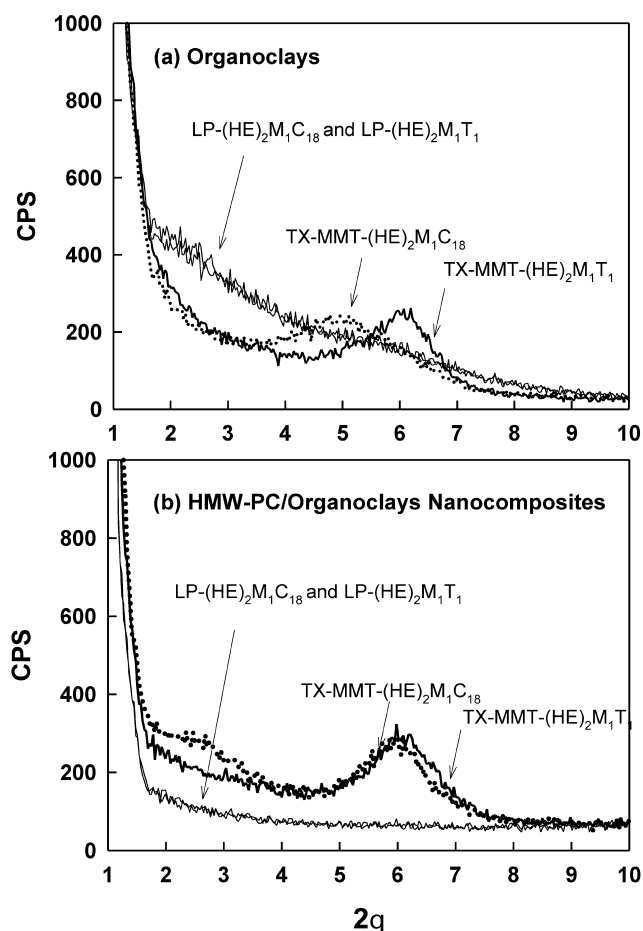


Fig. 10. Wide angle X-ray scattering results for (a) the pristine organoclays exchanged using Laponite<sup>®</sup> and TX-MMT with (HE)<sub>2</sub>M<sub>1</sub>C<sub>18</sub> and (HE)<sub>2</sub>M<sub>1</sub>T<sub>1</sub>, and (b) its HMW-PC nanocomposites.

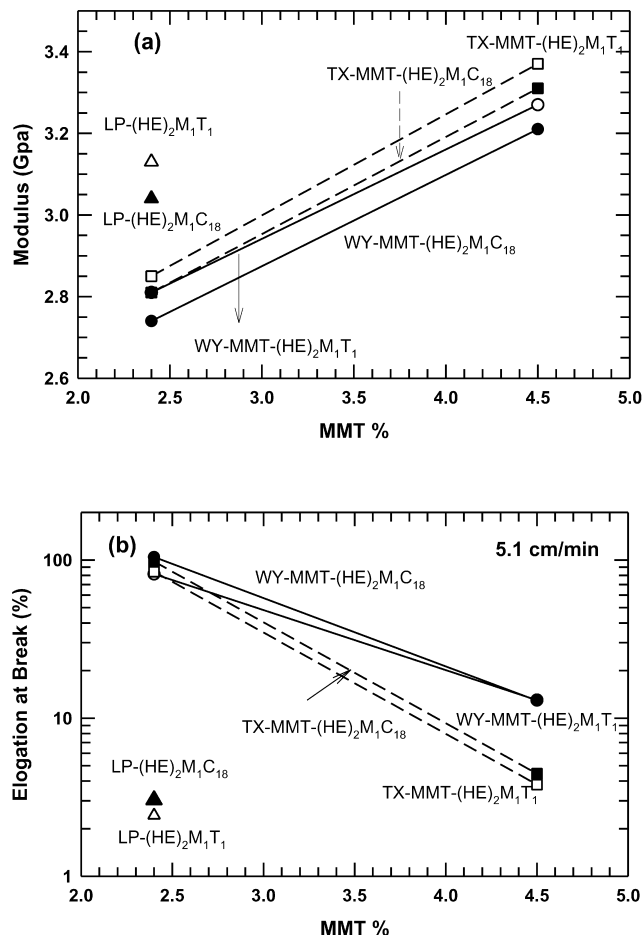


Fig. 11. Effects of clay type on (a) modulus and (b) elongation at break as a function of montmorillonite content for nanocomposites formed from HMW-PC with (HE)<sub>2</sub>M<sub>1</sub>C<sub>18</sub> (filled points) and (HE)<sub>2</sub>M<sub>1</sub>T<sub>1</sub> (open points) organoclays based on WY-MMT ((●), (○)), TX-MMT ((■), (□)), and Laponite<sup>®</sup> ((▲), (△)).

Molecular weight degradation of PC matrix was monitored by UV–Vis spectroscopy and intrinsic viscosity. Molecular weight degradation during melt processing produces phenolic end groups and strongly depends on the level of dispersion of the clay. Greater dispersion led to higher reduction molecular weight due to increased surface area of clay. Hydroxy-ethyl groups and tallow tails in the surfactant lead to more degradation. The level of thermal degradation was similar in the PC nanocomposites based on Laponite<sup>®</sup>, TX-MMT, and WY-MMT, which suggests that thermal degradation is less dependent on the type of clay used. Dynamic rheological properties support the trends of molecular weight degradation and dispersion of clay.

## Acknowledgements

This work was supported by the Air Force Office of Scientific Research, the Texas Advanced Technology

Program, and Mitsubishi Engineering Plastics Corp. The authors would like to thank Denis Ryan and Randy Chapman of Southern Clay Products for their help with color and X-ray analysis.

## References

- [1] Yoon PJ, Hunter DL, Paul DR. *Polymer* 2003;18:10.1016/S0032-3861(03)00523-8.
- [2] Fornes TD, Yoon PJ, Hunter DL, Keskkula H, Paul DR. *Polymer* 2002;43:5915–33.
- [3] Lee L. *J Polym Sci Part A* 1964;2:2859.
- [4] Davis A, Golden JH. *Makro Chem* 1964;78:16–23.
- [5] Davis A, Golden JH. *Nature* 1965;206:397.
- [6] Davis A, Golden JH. *J Chem Soc B* 1968;45–7.
- [7] Bratosiewicz RL, Booth C. *Eur Polym J* 1974;10:791–7.
- [8] Abbas KB. *Polymer* 1980;21:936–40.
- [9] Abbas KB. *Polymer* 1981;22:836–41.
- [10] Bailly C, Daumerie M, Legras R, Mercier JP. *Makromol Chem* 1986;187:1197–214.
- [11] McNeill IC, Rincon A. *Polym Degrad Stability* 1993;39:13–19.
- [12] Factor A. *Makromol Chemie* 1995;232:27–43.
- [13] Pulgisi C, Sturiale L, Montaudo G. *Macromolecules* 1999;32:2194–203.
- [14] Xie W, Gao Z, Pan W, Hunter D, Singh A, Vaia RA. *Chem Mater* 2001;13:2979–90.
- [15] Davis RD, Gilman JW, VanderHart DL. *Polym Degrad Stability* 2003;79:111–21.
- [16] Grim RE. *Clay mineralogy*. New York: McGraw-Hill; 1968.
- [17] Sperry JM, Peirce JJ. *Water Environ Res* 1993;71:316–22.
- [18] Smith WA, Barlow JW, Paul DR. *J Appl Polym Sci* 1981;26:4233–45.
- [19] Chen P. *Geology and mineralogy of the white bentonite beds of Gonzales county, Texas* 1968 Dissertation, University of Texas.
- [20] Cravero F, Keith KS, Murray HH, Toth T. *Appl Clay Sci* 2003;16:31–43.
- [21] Berger-Schunn A. *Practical color measurement: a primer for the beginner, a reminder for the expert*, Wiley and Sons, New York; 1994.
- [22] Billmeyer Jr FW. *Mater Res Stand* 1966;6:295–301.
- [23] Cho JW, Paul DR. *Polymer* 2001;42(3):1083–94.
- [24] Fornes TD, Yoon PJ, Keskkula H, Paul DR. *Polymer* 2001;42:9929–40. Fornes TD, Yoon PJ, Keskkula H, Paul DR. *Polymer* 2002;43:2121–2.
- [25] Shon K, Chang D, White JL. *Int Polym Process* 1999;(1):44–50.
- [26] Dennis HR, Hunter DL, Chang D, Kim S, White JL, Cho JW, Paul DR. *Polymer* 2001;42(23):9513–22.
- [27] ASTM E 313 Standard Practice for Calculating Yellowness and Whiteness Indices from Instrumentally Measured Color Coordinates, 2001.
- [28] Yoon PJ, Fornes TD, Paul DR. *Polymer* 2002;43:6727–41.
- [29] Shchori E, MaGrath JE. *J Appl Polym Sci Appl Polym Symp* 1978;34:103–17.
- [30] Tsuji T, Norisuye T, Fusjita M. *Macromolecules* 1974;7:178.
- [31] Kayano Y, Keskkula H, Paul DR. *Polymer* 1996;37:4505–18.
- [32] Krishnamoorti R, Vaia R, Giannelis EP. *Chem Mater* 1996;8:1728–34.
- [33] Krishnamoorti R, Giannelis EP. *Macromolecules* 1997;30:4097–102.
- [34] Solomon MJ, Almusallam AS, Seefeldt KF, Somwangthanaroj A, Varadan P. *Macromolecules* 2001;34:1864–72.
- [35] Ren J, Silva AS, Krishnamoorti R. *Macromolecules* 2000;33:3739–46.
- [36] Suh CH, White JL. *J Non-Newtonian Fluid Mech* 1996;62:175–206.
- [37] White JL. *Principles of polymer engineering of rheology*. New York: Wiley; 1990.
- [38] Yoon PJ, Han CD. *Macromolecules* 2000;33:2171–83.
- [39] Han CD, John MS. *J Appl Polym Sci* 1986;32:3809–40.
- [40] Alcover JF, Qi Y, Al-Mukhtar M, Bonnamy S, Bergaya F. *Clay Mineral* 2000;35:525–36.